ESC European Society of Cardiology
Cardiovascular Research
doi:10.1093/cvr/cvab165

Primary cilia control endothelial permeability by regulating expression and location of junction proteins

Mannekomba R. Diagbouga[1], Sandrine Morel [1,2], Anne F. Cayron [1,3,4], Julien Haemmerli[2], Marc Georges[2], Beerend P. Hierck [5], Eric Allémann[3,4], Sylvain Lemeille [1], Philippe Bijlenga [2], and Brenda R. Kwak [1]*

[1]Department of Pathology and Immunology, University of Geneva, Rue Michel-Servet 1, CH-1211 Geneva, Switzerland; [2]Neurosurgery Division, Department of Clinical Neurosciences, Geneva University Hospitals and University of Geneva, Rue Gabrielle-Perret-Gentil 4, CH-1211 Geneva, Switzerland; [3]School of Pharmaceutical Sciences, University of Geneva, Rue Michel-Servet 1, CH-1211 Geneva, Switzerland; [4]Institute of Pharmaceutical Sciences of Western Switzerland, University of Geneva, Rue Michel-Servet 1, CH-1211 Geneva, Switzerland; and [5]Department of Anatomy and Embryology, Leiden University Medical Center, Eindhovenweg 20, 2333ZC Leiden, the Netherlands

Received 18 June 2020; editorial decision 4 May 2021; accepted 9 May 2021; online publish-ahead-of-print 11 May 2021

Aims Wall shear stress (WSS) determines intracranial aneurysm (IA) development. Polycystic kidney disease (PKD) patients have a high IA incidence and risk of rupture. Dysfunction/absence of primary cilia in PKD endothelial cells (ECs) may impair mechano-transduction of WSS and favour vascular disorders. The molecular links between primary cilia dysfunction and IAs are unknown.

Methods and results Wild-type and primary cilia-deficient *Tg737*$^{orpk/orpk}$ arterial ECs were submitted to physiological (30 dynes/cm^2) or aneurysmal (2 dynes/cm^2) WSS, and unbiased transcriptomics were performed. *Tg737*$^{orpk/orpk}$ ECs displayed a five-fold increase in the number of WSS-responsive genes compared to wild-type cells. Moreover, we observed a lower trans-endothelial resistance and a higher endothelial permeability, which correlated with disorganized intercellular junctions in *Tg737*$^{orpk/orpk}$ cells. We identified ZO-1 as a central regulator of primary cilia-dependent endothelial junction integrity. Finally, clinical and histological characteristics of IAs from non-PKD and PKD patients were analysed. IAs in PKD patients were more frequently located in the middle cerebral artery (MCA) territory than in non-PKD patients. IA domes from the MCA of PKD patients appeared thinner with less collagen and reduced endothelial ZO-1 compared with IA domes from non-PKD patients.

Conclusion Primary cilia dampen the endothelial response to aneurysmal low WSS. In absence of primary cilia, ZO-1 expression levels are reduced, which disorganizes intercellular junctions resulting in increased endothelial permeability. This altered endothelial function may not only contribute to the severity of IA disease observed in PKD patients, but may also serve as a potential diagnostic tool to determine the vulnerability of IAs.

* Corresponding author. Tel: +41 22 379 5666, E-mail: Brenda.kwakchanson@unige.ch

Graphical Abstract

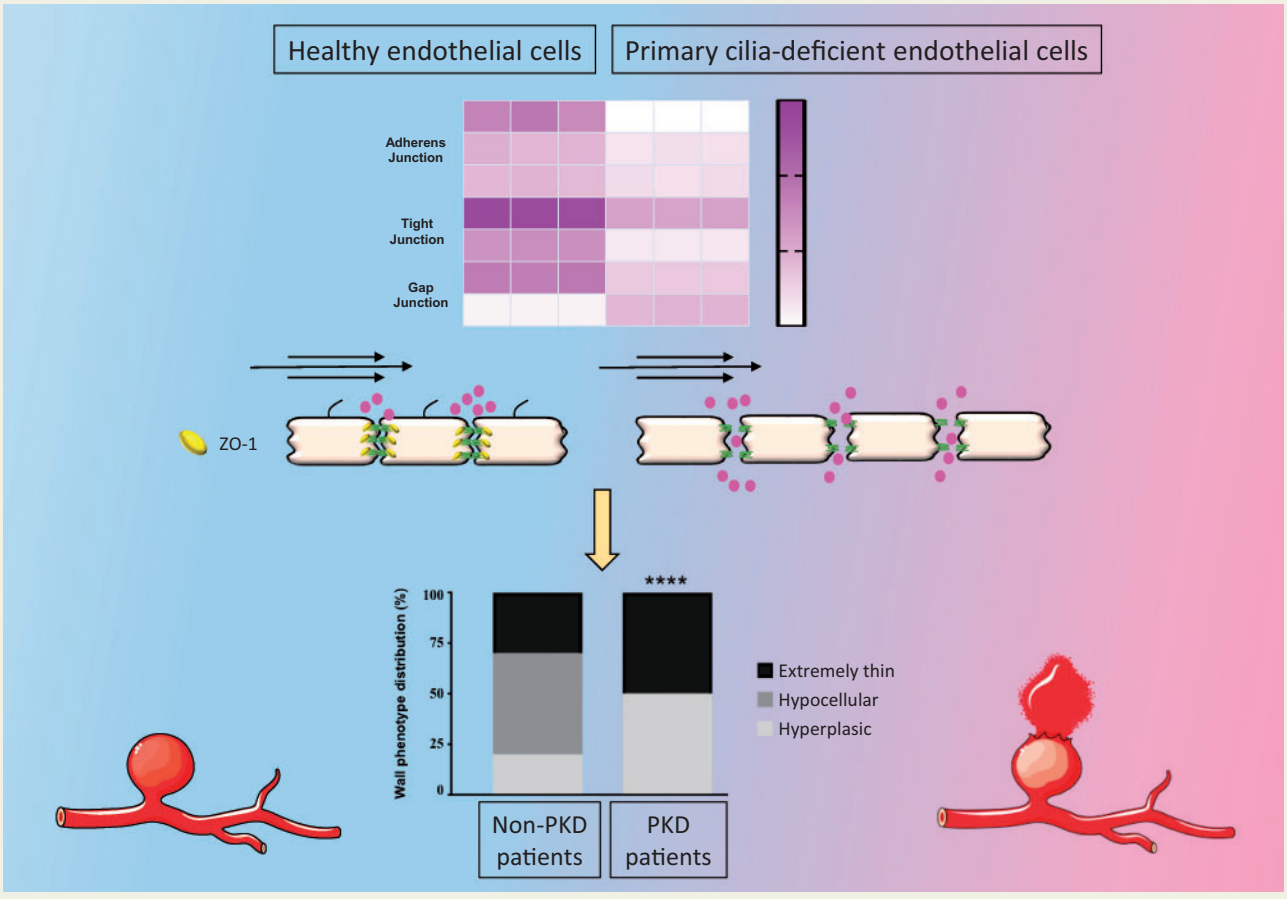

Keywords Intracranial aneurysm • Endothelial permeability • Primary cilium • Wall shear stress • Intercellular junctions

1. Introduction

Intracranial aneurysms (IAs) are local dilatations in cerebral arteries that predominantly develop at bifurcations in the circle of Willis, regions exposed to disturbed blood flow.[1,2] Rupture of an IA causes subarachnoid haemorrhage and is a life-threatening event. The treatment options to prevent IAs from rupturing are either surgical or endovascular and are both associated with important clinical risk as well.[1,2] IAs are characterized by a disrupted internal elastic lamina (IEL), dysfunction or loss of endothelial cells (ECs), inflammatory cell infiltration, extracellular matrix degradation, and loss of smooth muscle cells (SMCs).[3] The formation and growth of IAs is multifactorial, and wall shear stress (WSS) is a determinant factor.[4] A healthy endothelium is essential to maintain vascular integrity as it regulates vascular tone, thrombosis, and inflammatory events.[5] EC dysfunction is considered as the initiating event of IA disease.[2,4] Available evidence suggests that an excessively high WSS at bifurcations in the circle of Willis can trigger pro-inflammatory signalling in ECs that would stimulate leukocyte infiltration.[6] Recruited leukocytes secrete proteases, which enhance IEL disruption promoting the typical out-bulging of the arterial wall.[2–4] The processes inducing further growth of an IA are not yet fully understood. Interestingly, altered blood flow conditions in the IA lumen have been associated with progression of inflammation and degenerative changes of the aneurysm wall.[2–4] WSS controls vascular wall remodelling through mechano-sensors present at EC surface, including primary cilia.[2,5] Within the normal range of arterial flow, ECs release biochemical signals, which maintain the physiological function of these blood vessels.[5] Abnormal WSS or impaired mechanotransduction would trigger degenerative remodelling leading to an instable arterial wall prone to disease.[2] Indeed, patients with polycystic kidney disease (PKD) carrying a mutation in polycystin-1 (PC1) or polycystin-2 (PC2) genes that affects the expression or function of primary cilia are prone to vascular complications, such as hypertension, atherosclerosis, and IAs.[7] The prevalence of IAs in PKD patients ranges from 5% to 40%, and the rupture rate is five times higher than in the general population.[8]

Primary cilia are microtubule-based organelles found in most mammalian cell types that transmit microenvironmental clues into intracellular signals for molecular and cellular responses.[2] Correct assembly and maintenance of primary cilia relies on a wide range of proteins including intra-flagellar transport (IFT) proteins.[9] In the vasculature, endothelial primary cilia are essential for proper vascular development and

maintenance of structural integrity through calcium and nitric oxide signalling.[10] In adult mice, primary cilia are particularly abundant in ECs of arterial regions experiencing low WSS,[11] a condition that is typically observed in wide-neck IAs.[4] In agreement, EC-specific deletion of PC1, PC2, or IFT88 promotes IA development in mice.[12] We hypothesize that absence or dysfunction of primary cilia might either impair the adaptive EC response to low WSS or induce general structural changes in the endothelium, which compromise the integrity of the endothelial barrier and exacerbate the outcome of IA disease as seen in PKD patients. Here, we sought to investigate the molecular role of primary cilia in EC integrity using *in vitro* approaches. Finally, the results were compared with human IAs of the AneuX biobank.[13]

2. Methods

2.1 Cell culture and flow experiments

Previously established lines of embryonic aortic ECs from wild-type and *Tg737*$^{orpk/orpk}$ mice as well as *Tg737*$^{orpk/orpk}$ ECs stably transfected with Ift88-mCherry cDNA (*Tg737*$^{orpk/orpk}$–Ift88* ECs)[14] were used in this study. They were grown in dishes coated with 0.1% gelatin (Sigma-Aldrich) at 37°C in a humidified atmosphere containing 5% CO_2. Cells were cultured in Advanced DMEM (Gibco) supplemented with 2% foetal bovine serum (Sigma), 10 000 U/mL penicillin–streptomycin (Gibco), 1% glutamax (Gibco), and 1% insulin–transferrin–selenium (Gibco). Wild-type and *Tg737*$^{orpk/orpk}$ ECs were seeded at 30000 cells per channel in Ibidi µ-Slide VI$^{0.4}$ slides coated with 0.1% gelatin and grown till confluence. Cells were serum starved for 24 h prior exposure to flow. Laminar shear stress of 30 or 2 dynes/cm^2 was applied for 48 h using an Ibidi flow system.[15] For each set of flow experiments, control cells were kept under static conditions.

2.2 *Tjp1* knockdown

Wild-type ECs were transfected 24 h after seeding with ON-TARGETplus mouse *Tjp1* siRNA SMARTpool (Dharmacon) comprising individual siRNAs targeting the sequences CGAUAGUUAUGACG AAGAA, GAUGAAGGUUAGCGAGCAU, GCAGAGAGGAAGAGC GAAU, and UGGAAAUGAUGUCGGAAUA. Non-targeting (NT) siRNA was used as a control (Dharmacon). The transfections were performed in serum-free conditions using 25 nM siRNA and 4 µL DharmaFECT 4 transfection reagent. The *Tjp1*/zona occludens-1 (ZO-1) expression level was determined by quantitative RT–PCR (qPCR), immunofluorescence, and western blotting at 48 h post-transfection. Alternatively, stable *Tjp1* knockdown cells were obtained using the CRISPR-Cas9 system (GeneCopoeia). First, wild-type ECs were infected in medium containing 8 mg/mL of polybrene (0.2 µL) and lentiviral particles for Cas9 nuclease (LPP-CP-LYC9NU-10-100-CS) at MOI 10. At 6 h post-infection, the medium was changed and cells were selected with hygromycin (150 µg/mL) and FACS sorting. Secondly, selected cells were infected following the same protocol with *Tjp1* (LPPMC P274411L03-1-50) or scrambled (LPPCCPCTR01203-100-CS) sgRNA lentiviral particles at MOI 10, and cells were selected with puromycin (2 µg/mL) and FACS sorting. The ZO-1 expression level was determined using immunofluorescence and western blotting.

2.3 Trans-endothelial electrical resistance and permeability assays

Polyester membrane transwell inserts (6.5 mm diameter, 0.4 µm pore size, CoStar) were coated with 0.1% gelatin. Cells were grown on the apical side of the transwell insert until confluency. Trans-endothelial electrical resistance (TEER) of cell monolayers was assessed using an epithelial voltohmmeter (EVOM, World Precision Instrument). One electrode was placed in the upper compartment of the transwell and the second in the lower compartment. TEER ($\Omega.cm^2$) was calculated using the formula TEER = R × $area_{filter}$. Trans-endothelial permeability was assessed by the measurement of 4 kDa FITC-dextran passage across the cell monolayer. FITC-dextran was added to the apical side of the transwell, and the medium of the baso-lateral side was collected after 1, 4, and 6 h for analysis of the fluorescence intensity (excitation 485 nm, emission 525 nm, SpectraMax Paradigm, Molecular Devices). Control conditions included an empty gelatin-coated filter.

2.4 RNA extraction, reverse transcription, and quantitative PCR

Total RNA was isolated from cells using the nucleospin RNA II kit (Machery-Nagel) according to the manufacturers' instructions. The concentration of RNA was determined using a Nanodrop 2000c (ThermoFisher Scientific). Equal amounts of RNA were converted to cDNA using the QuantiTect Reverse Transcription Kit (Qiagen), and qPCRs were performed using ABI StepOne Plus detection system. We used Taqman gene expression assays (Applied Biosystems). The following primers were used: Tjp1 (Mm00493699_m1) and Gapdh (Mm99999915_g1) from ThermoFisher Scientific.

2.5 Protein quantification and western blot

Cell cultures were rinsed with PBS (pH = 7.4) and lysed in RIPA buffer (50 mmol/L Tris–HCl, 30 mmol/L NaCl, 1% NP40, 10 mmol/L NaF, 2 mmol/L Na_3VO_4, 1 mmol/L phenylmethylsulfonyl fluoride, complete protease inhibitor cocktail (Roche Applied Science), 1 mmol/L EDTA, 0.05% sodium dodecyl sulphate, 5 mmol/L sodium-deoxycholate, pH = 7.4). Cell lysates were gently mixed at 4°C for 20 min, and then spun at 13.500 rpm for 20 min to collect the supernatant. The concentration of the isolated proteins was determined using BCA Protein Assay Reagent (Thermo Scientific). About 10 µg of protein was separated by SDS–PAGE and electrophoretically transferred to PVDF membranes (Immobilon, Millipore). After 2 h blocking with 5% milk and 1% Tween in PBS, the membranes were incubated with primary antibodies recognizing ZO-1 (rabbit polyclonal, ThermoFisher Scientific, 1/250) or GAPDH (mouse monoclonal IgG, EMD Millipore, 1/30000). Thereafter, the appropriate secondary horseradish peroxidase-conjugated antibodies (Jackson ImmunoResearch; 1/5000) were used, followed by ECL detection (Millipore) using ImageQuant LAS4000 software. Band intensities were quantified using NIH Image software (NIH AutoExtractor 1.51; National Institutes of Health).

2.6 Immunofluorescence and immunohistochemistry

Cultured cells were fixed in ice-cold 100% methanol for 5 min, permeabilized with 0.2% Triton X-100 for 1 h, charges were neutralized with 0.5 mol/L NH_4Cl in PBS for 15 min, and cells were blocked for 30 min with 2% bovine serum albumin (AppliChem). Primary antibodies

recognizing acetylated α-tubulin (Mouse IgG2b, Sigma, 1/2000), ZO-1 (rabbit polyclonal, ThermoFisher Scientific, 1/50), ZO-2 (rabbit polyclonal, Cell signalling, 1/50), Catenin α-1 (rabbit polyclonal, Cell signalling, 1/200), Catenin β-1 (rabbit polyclonal, Cell signalling, 1/100), Claudin-3 (rabbit polyclonal, Abcam), and Connexin43 (rabbit polyclonal, Alpha diagnostic, 1/50) were diluted in blocking buffer and incubated with the samples overnight at 4°C. Finally, Alexa Fluor (488, 568)-conjugated goat anti-rabbit or goat anti-mouse antibodies (ThermoFisher Scientific, 1/2000) were used for signal detection. Nuclei and cytoplasm were counterstained with 4',6-diamidino-2-phenylindol (DAPI) and 0.003% Evans Blue, respectively. Samples were mounted with Vectashield (Vector Laboratories). Images were obtained with an epifluorescent Zeiss Axiocam microscope (Zeiss Axio Imager Z1) equipped with an AxioCam 506 mono camera (Carl Zeiss AG) or with an LSM800 Airyscan confocal microscope. Images were analysed using the software ZEN2.3 (Zeiss), and quantification was performed using the NIH Image software (NIH AutoExtractor 1.51; National Institutes of Health). For all junction proteins, the area of positive staining at the cell membrane and the total area were measured using ImageJ software. Results are given as the ratio of positive area/total area. In addition, intercellular junctions were classified for each cell from images by a blinded observer into predominantly sharp (thin, continuous), wide (thick, diffuse/scattered), or discontinuous (zigzag-like, with gaps) junctions (adapted from the reference16; Supplementary material online, *Figure S1* for examples). Cells of 15 images from three different experiments were quantified. For determination of the primary cilia incidence, parallel cultures of wild-type ECs on Ibidi slides were kept under static conditions or exposed to 30 or 2 dynes/cm^2. After 48 h, cultures were fixed and immunostained for acetylated α-tubulin to identify primary cilia. Primary cilia were counted in 50 images from five independent experiments by a blinded observer. The frequency of primary cilia under shear stress was normalized by the frequency under static conditions.

2.7 Human saccular IA samples

The University of Geneva @neurIST project aimed to collect prospectively and consecutively clinical, radiological, and pathological information of patients with IAs.[13] In this context, patients with newly diagnosed IA suffering from PKD were compared to non-PKD patients. Inclusion criteria were as follows: 1) new diagnosed IA between 2006 and 2017 on the basis of angiographic image (digital subtraction angiogram (DSA), magnetic resonance angiogram (MRA), or computed tomography with angiogram sequence (CTA)); 2) patients older than 18 years; 3) presence or not of an already diagnosed PKD; and 4) acceptance and signature of consent forms. Demographic and clinical parameters such as age at diagnosis, sex, smoking status, hypertension status, and positive familial history were analysed. All radiological parameters were taken from angiogram-type DSA, MRA, or CTA as part of preoperative planning or clinical follow-up. The presence of unique or multiple IAs, and the location of the aneurysm were noted. Locations were defined as follows: internal carotid artery (ICA, including ophthalmic, anterior choroid, and bifurcation), anterior communicating artery (Acom), middle cerebral artery (MCA, including M1-segment, bifurcation, and M2-segment), posterior communicating artery (Pcom), pericallosal artery, and posterior circulation (Post.Cir, including posterior inferior cerebellar artery, basilar and its branches, posterior cerebral artery).

For histological studies, the human saccular IA samples at the MCA were retrieved from the Swiss AneuX biobank.[13] Briefly, IA domes after clipping were fixed in formol, embedded in paraffin, and 5 µm sections were used for histology analysis. IA domes were stained for haematoxylin and eosin, Masson-trichrome (total collagen), Victoria blue (elastin), and picrosirius red (type I and III collagen, Sigma-Aldrich). Immunohistochemistry was performed on IA dome sections using antibodies recognizing α-SMA (mouse IgG2a antibody, clone 1A4,[17] 1/100; a general marker of SMCs), CD68 (mouse IgG1 antibody, clone KP1, Dako, 1/200; a marker of macrophages), CD31 (rabbit polyclonal antibody, clone pAK, Dianova, 1/25; a marker of ECs), ZO-1 (rabbit polyclonal, ThermoFisher Scientific, 1/100), and VE-cadherin (rabbit polyclonal, Abcam, 1/500). Before using the first antibody, immunoreactivity was retrieved by microwave treatment (600 W, 5 min) in citrate buffer (10 mM, pH = 6.0) for α-SMA and CD68, and by pressure cooker treatment (3 min) in citrate buffer for CD31, ZO-1, and VE-cadherin. Goat anti-mouse or anti-rabbit biotinylated IgGs (Dako) were used as secondary antibodies and the streptavidin–biotin peroxidase complex and 3,3′-diamino-benzidine chromophore were used for visualization (EnVision system; Dako). Hemalun (Merck) was used as counterstaining. All stainings were performed on consecutive sections.

This study is in accordance with the Helsinki Declaration of the World Medical Association and was approved by the Ethical Committee of the Geneva University Hospitals, Geneva, Switzerland, as part of the @neurIST study (Geneva State Ethics Commission for Research PB_2018-0073 previously NAC 07-056). All patients signed the consent forms and approved for the use of their data and biological samples in the field of cerebrovascular research.

2.8 Library preparation, sequencing, read mapping to the reference genome, and gene coverage reporting

RNA was isolated from ECs after exposure to flow, as described above. Three experiments for each condition were performed. The quality of all samples was verified using the Agilent 2100 Bioanalyzer with the Agilent RNA 6000 Nano Kit (Agilent Technologies). cDNA libraries were constructed by the genomic platform of the University of Geneva using the Illumina TruSeq RNA sample preparation kit according to the manufacturers' protocol. Libraries were sequenced using single-end (50-nt-long) on Illumina HiSeq2000. FastQ reads were mapped to the ENSEMBL reference genome (GRCm38.80) using STAR version 2.4.0j[18] with standard settings, except that any reads mapping to more than one location of the genome (ambiguous reads) were discarded ($m = 1$). A unique gene model was used to quantify reads per gene. In short, the model considers all annotated exons of all annotated protein-coding isoforms of a gene to create a unique gene where the genomic region of all exons was considered as coming from the same RNA molecule and merged together.

2.9 RNAseq data analysis

All reads overlapping the exons of each unique gene model were reported using featureCounts version 1.4.6-p1.[19] Gene expression was reported as raw counts and in parallel normalized in reads per kilobase million (RPKM) in order to filter out genes with low expression value (1 RPKM) before calling for differentially expressed genes. Library size normalizations and differential gene expression calculations have been performed using the package edgeR[20] designed for the R software.[21] Only genes having a significant fold change ≥3 and the Benjamini–Hochberg corrected *P*-value of <0.001 were considered for the differentially expressed genes analysis. Variation between samples was measured using a multidimensional scaling plot. Differentially expressed genes were annotated based on the PANTHER tool gene ontology: protein class

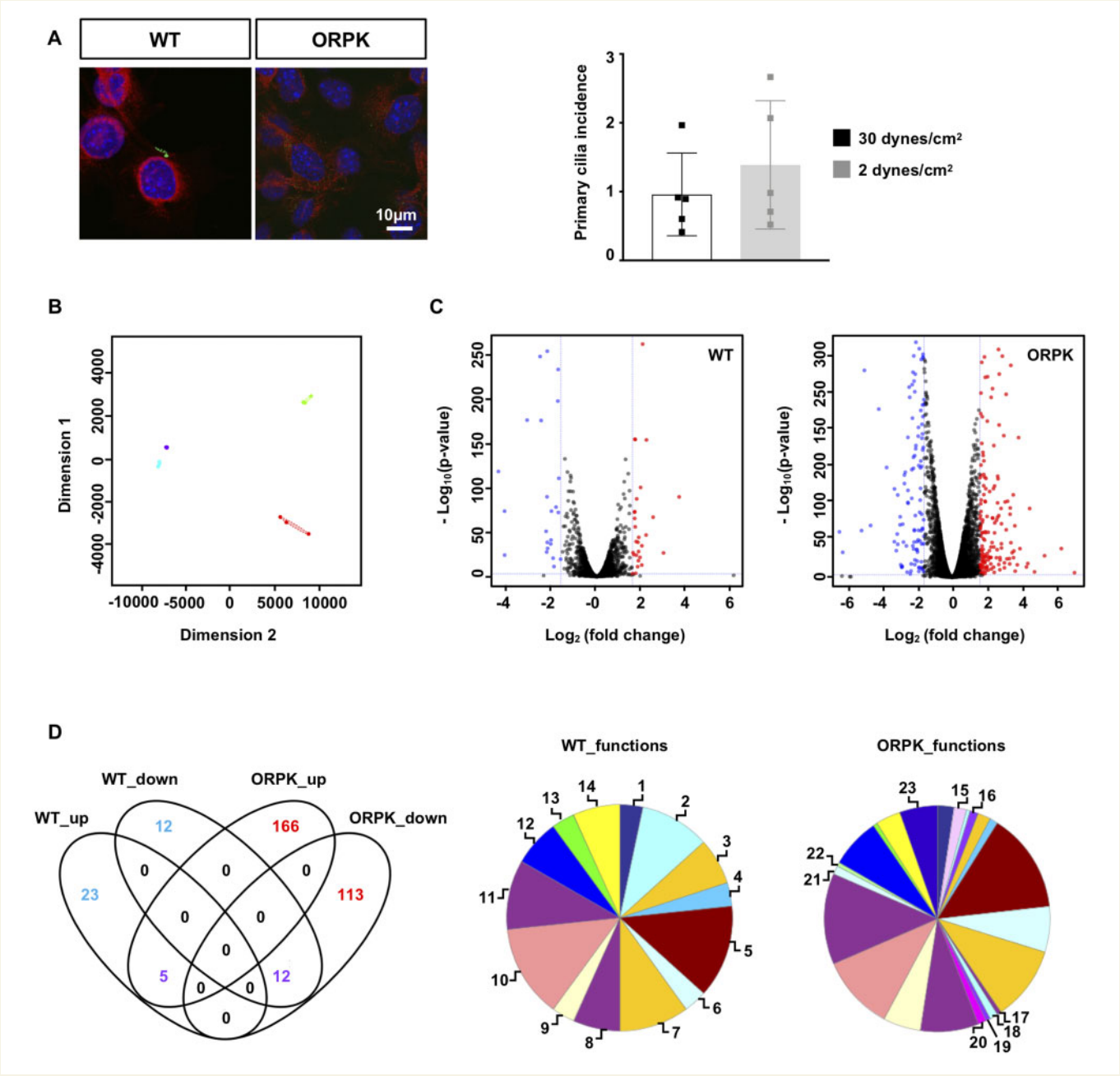

Figure 1 Primary cilia regulate gene expression in response to aneurysmal flow. (*A*) Acetylated α-tubulin staining for primary cilia (green) in wild-type (WT) and *Tg737*$^{orpk/orpk}$ (ORPK) ECs. Nuclei were stained with DAPI (blue), and cells were counterstained with Evans blue (red). Quantification of primary cilia in WT ECs after 48h exposure to a WSS of 30 or 2 dynes/cm^2. Mean ± SD; unpaired *t*-test. Results are obtained from five independent experiments. (*B*) Multidimensional scaling plot representing similarities in gene expression between WT and ORPK ECs. WT: violet = 30 dynes/cm^2, blue = 2 dynes/cm^2. ORPK: green = 30 dynes/cm^2, red = 2 dynes/cm^2. Results are obtained from three independent experiments. (*C*) Volcano plot displaying differential expressed genes under 2 dynes/cm^2 *vs.* 30 dynes/cm^2 in WT and ORPK ECs. Red and blue dots represent the up- and down-regulated genes, respectively. (*D*) Venn diagram showing the number of WSS-induced differentially expressed genes in WT and ORPK ECs. Colours represent differentially expressed genes in presence (blue), absence (red), or independent (purple) of primary cilia. Pie charts of differentially expressed genes in WT and ORPK ECs based on Gene Ontology functional protein class. 1 = calcium binding; 2 = cell junctions; 3 = cytoskeletal; 4 = defence/immunity; 5 = enzyme modulators; 6 = extracellular matrix; 7 = hydrolases; 8 = nucleic acid binding; 9 = oxidoreductases; 10 = receptors; 11 = signalling molecules; 12 = transcription factors; 13 = transfer/carriers; 14 = transferases; 15 = cell adhesion; 16 = chaperones; 17 = isomerases; 18 = ligases; 19 = lyases; 20 = membrane trafficking; 21 = storage; 22 = structural; 23 = transporters.

and represented in pie charts. 1: Calcium-binding proteins (PC00060); 2: Cell junction proteins (PC00070); 3: Cytoskeletal proteins (PC00085); 4: Defence/immunity proteins (PC00090); 5: Enzyme modulators (PC00095); 6: Extracellular matrix proteins (PC00102); 7: Hydrolases (PC00121); 8: Nucleic acid binding proteins (PC00171); 9: Oxidoreductases (PC00176); 10: Receptors (PC00197); 11: Signalling

molecules (PC00207); 12: Transcription factors (PC00218); 13: Transfer/carrier proteins (PC00219); 14: Transferases (PC00220); 15: Cell adhesion molecules (PC00069); 16: Chaperones (PC00072); 17: Isomerases (PC00135); 18: Ligases (PC00142); 19: Lyases (PC00144); 20: Membrane traffic proteins (PC00150); 21: Storage proteins (PC00210); 22: Structural proteins (PC00211); 23: Transporters (PC00227). Furthermore, genes coding for intercellular junction proteins were selected and categorized per junction type using the cut-off value of 15 RPKM, and a fold change of ≥1.5. Heatmaps were generated in GraphPad prism 8.0.1.

2.10 Statistical analysis

All data analyses were done with GraphPad Prism 8.0.1 software, except for the analysis of human IA location, which has been performed with RStudio® (Version 1.3.1093). Results are shown in mean ± SD, in median (interquartile range, IQR), in percentage, or in odds ratio (95% CI). Comparisons of means have been performed using Student's *t*-test. Comparisons of medians, distributions, or percentages have been performed using non-parametric Mann–Whitney *U*-test, Fisher's exact test, and chi-square test, respectively. Data were considered statistically significant at $P \leq 0.05$: $^{*}P \leq 0.05$, $^{**}P \leq 0.01$, $^{***}P \leq 0.001$, and $^{****}P \leq 0.0001$.

3. Results

3.1 *Tg737*$^{orpk/orpk}$ ECs display a larger number of WSS-responsive genes

The transgenic mouse model *Tg737*$^{orpk/orpk}$ with a mutation in Tg737/IFT88 has been largely used to decrypt the role of primary cilia.[10,14] Wild-type and *Tg737*$^{orpk/orpk}$ ECs were stained for primary cilia using antibodies against acetylated α-tubulin. As expected, wild-type ECs exhibit primary cilia, and no such structures were detected in *Tg737*$^{orpk/orpk}$ ECs (*Figure 1A*). Then, ECs were exposed for 48 h to physiological WSS (30 dynes/cm^2) or aneurysmal low WSS (2 dynes/cm^2), and the number of primary cilia was counted. The percentage of cells containing primary cilia was not different after 48 h of either level of WSS (*Figure 1A*), indicating that our EC culture model with wild-type and *Tg737*$^{orpk/orpk}$ cells will allow us to decipher the role of endothelial primary cilia in the response to flow. Next, we performed unbiased transcriptomics (RNAseq) and compared gene expression level at 30 and 2 dynes/cm^2 in wild-type and *Tg737*$^{orpk/orpk}$ ECs. Visualizing the data on a multidimensional scaling plot (*Figure 1B*) illustrates the divergence in response to WSS between ECs with and without primary cilia. Indeed, wild-type ECs under different levels of WSS show a high degree of similarity, whereas *Tg737*$^{orpk/orpk}$ ECs represent much more variation of gene expression in response to WSS. Actually, *Tg737*$^{orpk/orpk}$ ECs show approximately a fivefold increase in the number of WSS-responsive genes compared to wild-type ECs (*Figure 1C*). The comparison of physiological flow to pathological flow identified 28 and 24 up- and down-regulated genes (Supplementary material online, *Table S1*) in wild-type ECs. The same comparison in *Tg737*$^{orpk/orpk}$ ECs yielded 171 and 125 up- and down-regulated genes (Supplementary material online, *Table S2*). As illustrated in the Venn diagram of *Figure 1D*, 17 differentially expressed genes in wild-type ECs, in response to aneurysmal flow, overlapped with differentially expressed genes in *Tg737*$^{orpk/orpk}$ ECs indicating that they are regulated independently of the presence of primary cilia. Moreover, 35 genes were uniquely affected by pathological flow in presence of cilia and 279 genes were uniquely affected by this flow in absence of cilia.

To further understand the biological functions of these uniquely differentially expressed genes, we performed a protein class functional annotation. Predictably, the *Tg737*$^{orpk/orpk}$ genes were spread into more groups than wild-type genes with varying distributions of protein classes amongst the two cell types (*Figure 1D*). For example, 10.0%, 3.3%, and 6.7% of genes in wild-type cells were involved in cell junctions, extracellular matrix, and cytoskeletal regulation, respectively, as compared to 0.6%, 6.5%, and 1.8% in *Tg737*$^{orpk/orpk}$ cells. Altogether, our results show that the lack of primary cilia increases the sensitivity of ECs to low WSS and that genes important for arterial wall structure are affected.

3.2 *Tg737*$^{orpk/orpk}$ endothelium exhibits low barrier integrity and perturbed junctions

An intact endothelial barrier is important for the integrity of the vascular wall.[5] Therefore, we investigated the barrier properties of wild-type and *Tg737*$^{orpk/orpk}$ EC monolayers by two different methods, that is TEER and trans-endothelial permeability. Monolayers of wild-type ECs exhibited a TEER of about 80 Ohm.cm^2. TEER was reduced in *Tg737*$^{orpk/orpk}$ ECs to 50 Ohm.cm^2, a value that was close to the resistance of the empty filters (i.e. 40 Ohm.cm^2) (*Figure 2A*). As expected, trans-endothelial permeability of 4 kDa FITC-dextran in wild-type EC monolayers displayed a progressive increase between 1, 4, and 6 h. The permeability of the fluorescent tracer was threefold larger in *Tg737*$^{orpk/orpk}$ EC monolayers (*Figure 2B*). Together, these results show decreased endothelial barrier properties in ECs without primary cilia.

The integrity of the endothelial barrier is critically regulated by different protein families at the interface between ECs, forming tight junctions (TJs), adherens junctions (AJs), and gap junctions (GJs) at cell–cell contacts.[22] Altered expression or organization of these junction proteins would result in endothelial barrier disruption and increased trans-endothelial permeability. The transcripts of the TJ genes *Claudin3* (*Cldn3), Cldn9, Cldn12, Tight junction protein1* (*Tjp1;* encoding ZO-1), *Tjp2* (encoding ZO-2), and *Junction adhesion molecule1* (*Jam1)* were reduced in *Tg737*$^{orpk/orpk}$ ECs, whereas *Jam3* transcripts were increased in *Tg737*$^{orpk/orpk}$ ECs compared to wild-type ECs (*Figure 2C*). The transcripts of the AJ genes *Cadherin3 (Cdh3), Cdh6, Cdh16, Catenin α-1* (*Ctnna1*), *Catenin α like-1 (Ctnnal1), Catenin β like-1 (Ctnnbl1),* and *Nectin2 (Pvrl2)* were decreased, whereas the expression of *Cdh11, Catenin β-1 (Ctnnb1),* and *Catenin δ-1 (Ctnnd1)* mRNA was larger in *Tg737*$^{orpk/orpk}$ ECs (*Figure 2C*). The endothelial GJ transcripts *Gja1* (encoding Cx43) and *Gjc1* showed an inverse expression pattern in wild-type and *Tg737*$^{orpk/orpk}$ ECs with the expression of *Gja1* being highest in *Tg737*$^{orpk/orpk}$ ECs (*Figure 2C*). mRNAs of other junction-associated genes such as *Desmoplakin* (*Dsp*), *Junction Plakoglobin* (*Jup*), *Plakophilin2* (*Pkp2), Pkp4, Pinin* (*Pnn*), and *Periplakin* (*Ppl*) were all less expressed in *Tg737*$^{orpk/orpk}$ compared to wild-type ECs (*Figure 2C*). The differences in transcript levels of these TJ, AJ, and GJ proteins between wild-type and *Tg737*$^{orpk/orpk}$ ECs were persistent under physiological and aneurysmal WSS (Supplementary material online, *Figure S2*). In agreement with the results obtained at the transcript level, *Tg737*$^{orpk/orpk}$ ECs expressed less ZO-1, ZO-2, Catenin α-1, Claudin-3, and more Cx43 protein in comparison to wild-type ECs (*Figure 2D*). In addition to these differences in expression level, junction proteins in *Tg737*$^{orpk/orpk}$ ECs displayed a scattered organization at cell–cell contacts. Altogether, these experiments show that the *Tg737*$^{orpk/orpk}$ endothelium exhibits reduced barrier integrity and perturbed intercellular junctions.

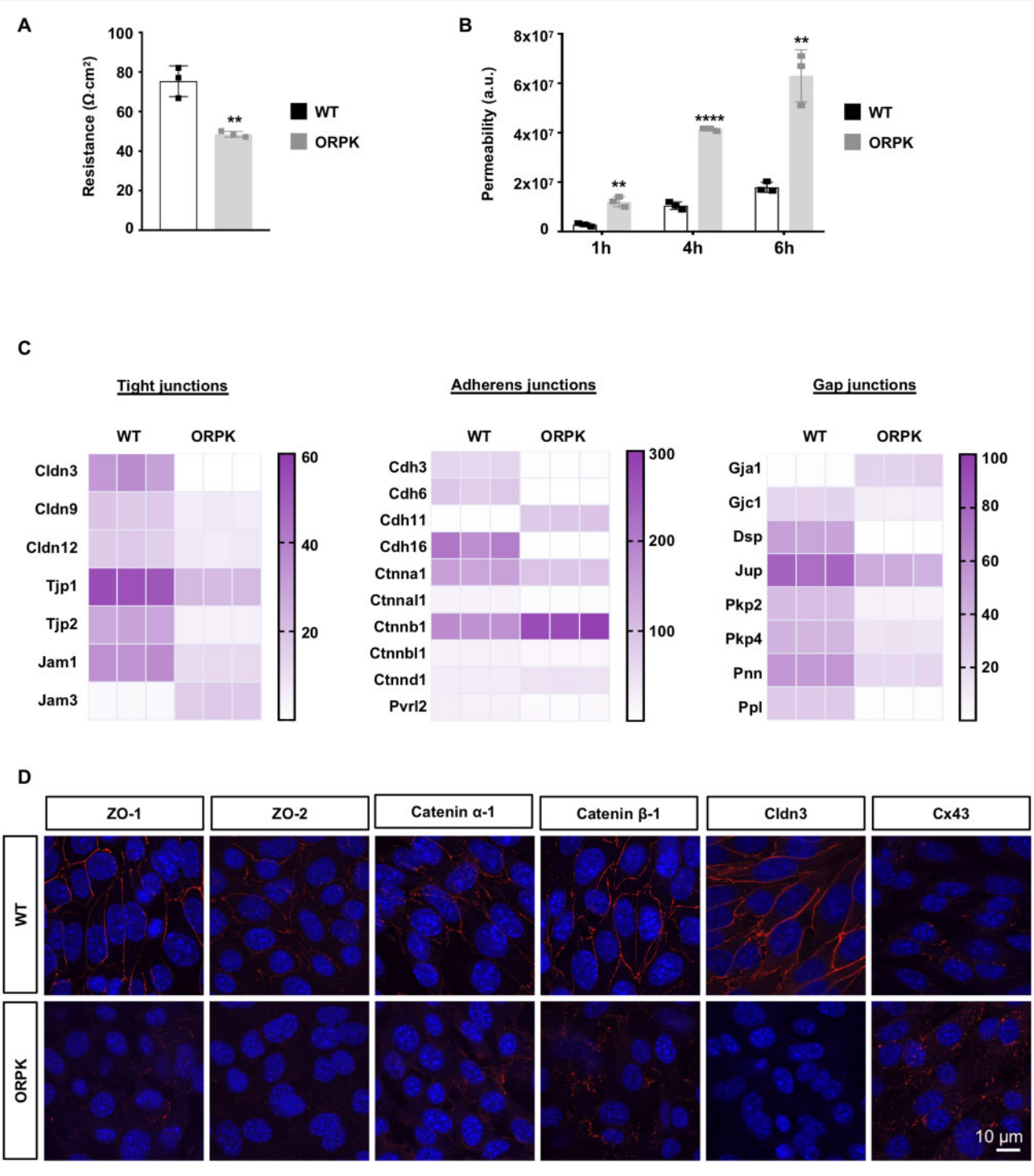

Figure 2 Primary cilia regulate EC barrier integrity and junction protein expression. (*A*) Trans-endothelial resistance in WT and ORPK ECs. Mean ± SD. Results are obtained from three independent experiments (in duplicate for each experiment). (*B*) Trans-endothelial permeability assay in WT and ORPK ECs. Mean ± SD. Results are obtained from three independent experiments (in duplicate for each experiment). (*C*) Heatmaps comparing expression levels of TJ, AJ, GJ, and associated desmosomal-family genes in WT and ORPK ECs. Gene expression levels are represented in RPKM. Represented genes are ≥15 RPKM in at least one condition, with a fold change ≥1.5 between WT and ORPK ECs. (*D*) Immunofluorescent staining (in red) of ZO-1, ZO-2, Catenin α-1, Catenin β-1, Cldn3, and Cx43 on confluent cultures of WT and ORPK ECs. Nuclei were stained with DAPI (blue). $^{**}P \leq 0.01$; $^{****}P \leq 0.0001$. Comparison of means has been performed using unpaired *t*-test.

3.3 Silencing ZO-1 modifies the arrangement of junction proteins

TJ, AJ, and GJ complexes consist of specific molecules at the junction and intracellular interacting proteins that mediate their distinctive functions but also share common components through their interaction with the cytoskeleton (Supplementary material online, *Figure S3*).[22] As ZO-1 binds to important protein components of TJs (e.g. claudins), AJs (e.g. Catenins), and GJs (e.g. Cx43), we have first studied the role of this shared protein in junction organization and permeability. *Tjp1* mRNA and ZO-1 expression was reduced in wild-type ECs transfected with siTjp1 compared with NT siRNA (*Figure 3A*). Importantly, knock-down of ZO-1 expression in ECs induced important alterations in the expression and subcellular location of other junction proteins. Similar to the *Tg737*$^{orpk/orpk}$ ECs, we observed a lower expression of ZO-2 and Claudin-3, and a trend towards increased expression of Cx43. Moreover, ZO-1 knock-down leads to significant differences in the junctional arrangement of ZO-2, Catenin α-1, Catenin β-1, Claudin-3, and Cx43 into a wider and more discontinuous direction (*Figure 3B and C*). Finally, we found that TEER was lower in ECs with knock-down of *Tjp1* as compared to control ECs transduced with a scrambled sequence. Likewise, the FITC-Dextran permeability was increased by twofold in *Tjp1* knock-down EC monolayers at 4 and 6 h (*Figure 3D*). Together, these results indicate that ZO-1 plays a key role in regulation of the integrity of the endothelium.

3.4 Rescue of primary cilia enhances ZO-1 and junction integrity

To further investigate the mechanistic link between loss of primary cilia and reduced ZO-1, we used *Tg737*$^{orpk/orpk}$ ECs stably transfected with Ift88-mCherry cDNA (*Tg737*$^{orpk/orpk}$–Ift88* ECs). As shown previously,[14] rescue of Ift88 in *Tg737*$^{orpk/orpk}$ ECs induced a structural recovery of primary cilia. Rescue of primary cilia not only induced an important increase in ZO-1 expression but also resulted in a sharper junctional arrangement of the protein in *Tg737*$^{orpk/orpk}$–Ift88* ECs (*Figure 4A and B*). These changes in ZO-1 were accompanied by increased expression of Catenin α-1 and Catenin β-1. Moreover, the junctional arrangement of ZO-2, Catenin α-1, and Catenin β-1 was improved in *Tg737*$^{orpk/orpk}$–Ift88* ECs. However, rescue of primary cilia did not affect Claudin-3 and Cx43 expression levels nor did it exert beneficial effects onto the junctional arrangement of Cx43 (*Figure 4A and B*). Finally, we found a rescue of primary cilia modestly improved TEER in *Tg737*$^{orpk/orpk}$–Ift88* ECs (*Figure 4C*). Together, these results indicate that by affecting ZO-1 expression and/or subcellular location primary cilia play a key role in the structural arrangement of cell–cell junctions.

3.5 IAs in patients affected or not by PKD

To test whether impaired function or absence of primary cilia would affect endothelial ZO-1 expression and IA wall organization, we compared IAs from PKD and non-PKD patients. All @neurIST demographic and clinical data are presented in *Table 1*. Between 2006 and 2017, 925 patients were enrolled with a new IA (1076 IAs). In the cohort, 21 patients (2.3%) with 45 IAs were either previously diagnosed with PKD or under nephrological follow-up. Aneurysms were found in absence of a PKD diagnosis in 904 patients (97.7%). Age, sex, and smoking status were not different between PKD and non-PKD groups. As expected, PKD patients reported more frequently a positive familial history of IAs, hypertension, and multiple aneurysms than control patients. However, IAs were more frequently located in the middle cerebral artery (MCA) territory in the PKD group (51.1%) compared to the non-PKD group (34.8%, $P = 0.037$) (*Figure 5A*). Next, human IA domes located on the MCA were extracted from the Swiss AneuX biobank, and histological analysis was performed.[13] Patient and IA characteristics are shown in *Table 2*. IAs of PKD patients appeared smaller, which is probably due to the fact that in PKD patients IAs are promptly treated. Importantly, IAs of PKD patients were taken from the same location, and IA bottleneck factors were comparable to the ones of control patients, suggesting that they might have been submitted to similar WSS. We measured IA vessel wall area and showed that in PKD patients IAs were thinner compared to non-PKD IAs (*Figure 5B*). No differences were found between PKD and non-PKD IAs in SMC, macrophage, and elastin content (data not shown). However, PKD IAs contained less total collagen than non-PKD IAs, and the relative contribution of type I and III collagen was different with more type I collagen and less type III collagen in PKD IAs (*Figure 5C*). Next, we classified the IA domes in four grades of severity based on previously defined histological characteristics[13,23]; that is endothelialized wall with linearly organized SMCs (Grade A), thickened wall with disorganized SMCs (Grade B), hypocellular wall with either intimal hyperplasia or organizing luminal thrombus (Grade C), or extremely thin thrombosis-lined hypocellular wall (Grade D). IA domes from PKD patients showed increased frequency of the most severe phenotype (Grade D) as compared to non-PKD IA domes (*Figure 5C*). Next, we assessed ZO-1 expression in ECs of IA domes of PKD and non-PKD patients. A superficial temporal artery with well-preserved ECs was used to support the validity of the immunostaining (Supplementary material online, *Figure S4*). Immunostaining with the endothelial marker CD31 revealed that the majority of IAs displayed a partial loss of ECs, as expected. Interestingly, ZO-1 expression level was reduced in ECs of PKD than non-PKD IA domes (*Figure 5D*). Indeed, ZO-1 staining in ECs of non-PKD domes presented as a signal of almost 4 µm, a value that was reduced by 33% in PKD domes. Likewise, the junctional protein VE-cadherin tended to display reduced immunosignal in PKD domes (*Figure 5E*). Taken together, our results show that even if PKD IA domes were smaller, they displayed a severe IA wall degradation and the remaining ECs in the aneurysm dome exhibit a lower ZO-1 content.

4. Discussion

Primary cilia absence or dysfunction in PKD patients has been associated with increased IA formation and progression.[1,12] The molecular mechanism by which primary cilia promote IA disease is however not yet understood. Here, we investigated the role of mechano-sensitive primary cilia on EC function in the context of IA disease. Using *in vitro* flow experiments (48 h) and an unbiased transcriptomic approach, we showed that the loss of primary cilia in ECs was associated with a fivefold increase in the number of WSS-responsive genes (*Figure 1*), indicating that primary cilia in ECs may have a dampening effect on the pathological response to aneurysmal low WSS. Furthermore, we demonstrated that primary cilia-deficient ECs had a reduced barrier integrity that was concomitant with disrupted junction proteins such as ZO-1, ZO-2, Catenin α-1, Catenin β-1, Cx43, and Claudin-3 (*Figure 2*). Reducing ZO-1 in wild-type ECs altered the organization of TJ, AJ, and GJ proteins, generated a drop in TEER, and an increase in endothelial permeability, pointing to a central role of ZO-1 for a proper endothelial barrier function (*Figure 3*). Moreover, rescue of primary cilia in ECs resulted in improved ZO-1 expression and junctional organization (*Figure 4*). IA domes from PKD patients had thinner walls with a lower collagen content, as well as a shift

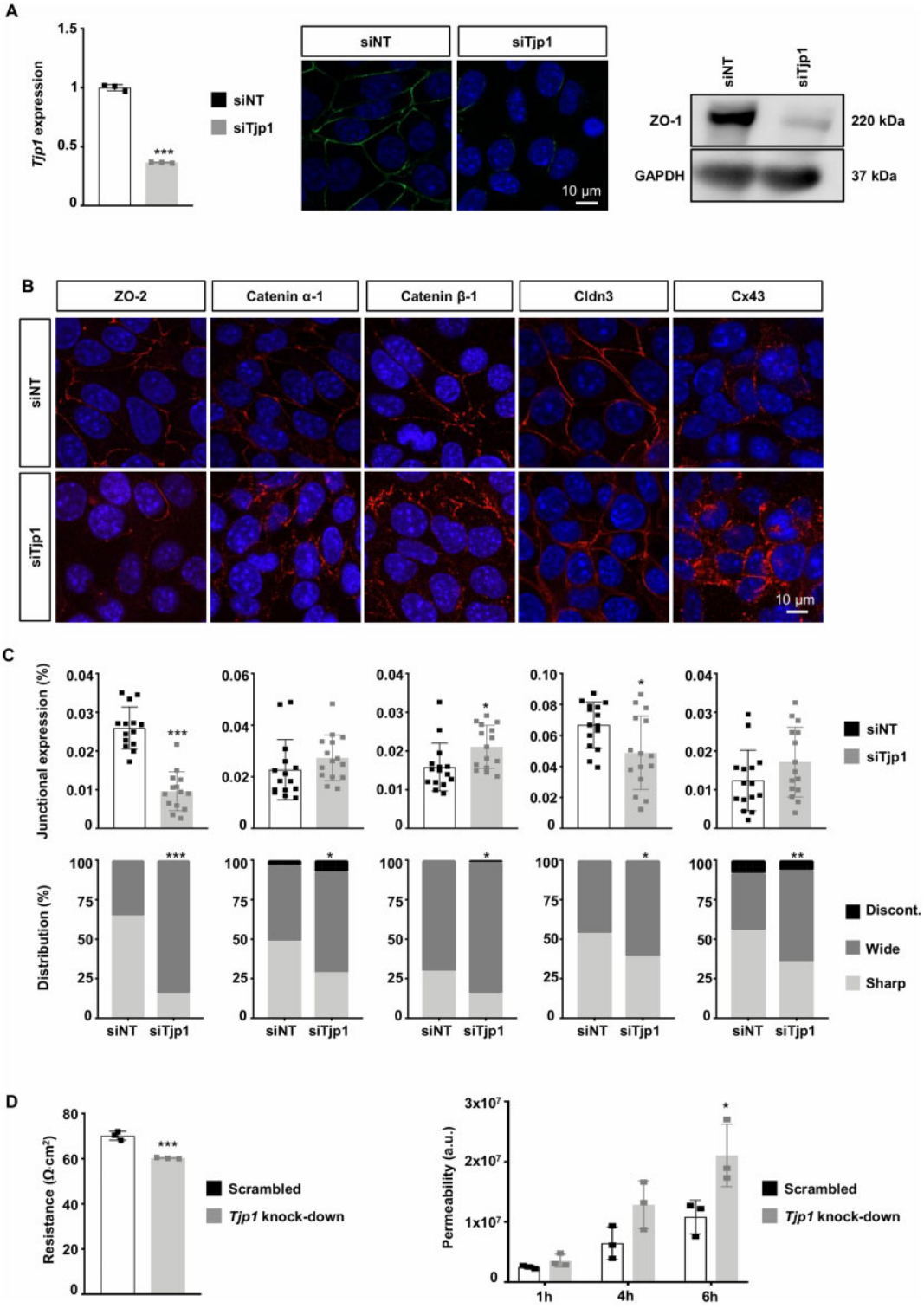

Figure 3 *Tjp1* knockdown regulates expression and organization of junction proteins. (*A*) *Tjp1*/ZO-1 expression in WT ECs transfected with *Tjp1* or NT siRNA assessed by qPCR (left), immunofluorescence (middle), and western blot (right). Mean ± SD. Results are obtained from three independent experiments. For qPCR samples, triplicates were used. (*B*) Immunofluorescent staining (in red) of ZO-2, Catenin α-1, Catenin β-1, Cldn3, and Cx43 on confluent cultures of WT ECs transfected with *Tjp1* or NT siRNA. Nuclei were stained with DAPI (blue). (*C*) Quantification of *B* for fluorescence intensity (top) or junction organization (bottom). Mean ± SD (top) or distribution (%; bottom). Results are obtained from quantification of four to five images in three independent experiments. (*D*) Trans-endothelial resistance or permeability in *Tjp1* knock-down or control (scrambled) ECs. Mean ± SD. Results are obtained from three independent experiments (in duplicates). $^{*}P \leq 0.05$; $^{**}P \leq 0.01$; $^{***}P \leq 0.001$. Comparison of means and distributions has been performed using unpaired *t*-test and chi-square test, respectively.

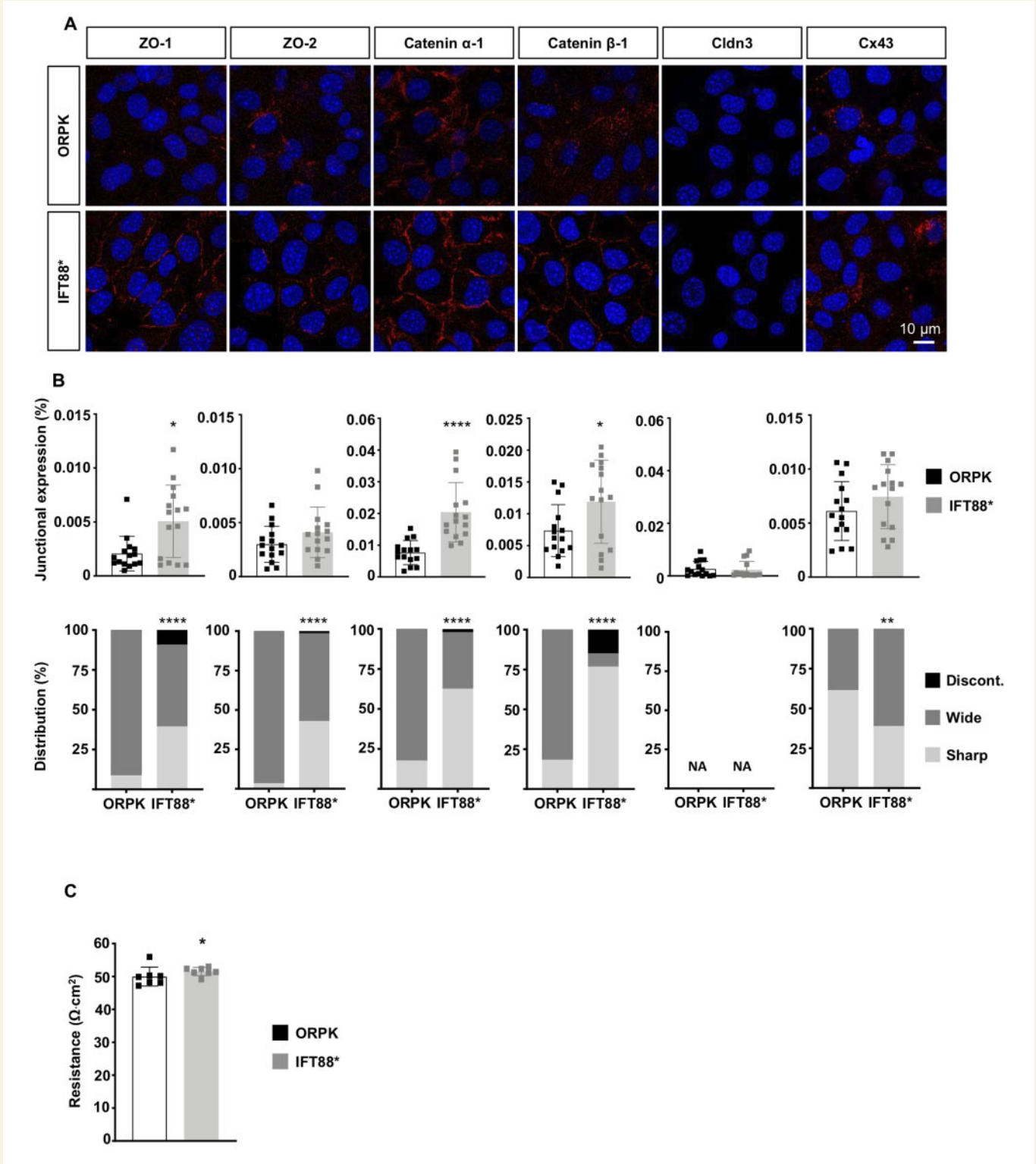

Figure 4 Rescue of primary cilia improves ZO-1 expression and junctional arrangement. (*A*) Immunofluorescent staining (in red) of ZO-1, ZO-2, Catenin α-1, Catenin β-1, Cldn3, and Cx43 on confluent cultures of ORPK and *Tg737*$^{orpk/orpk}$–Ift88* (IFT88*) ECs. Nuclei were stained with DAPI (blue). (*B*) Quantification of *A* for fluorescence intensity (top) or junction organization (bottom). Mean ± SD (top) or distribution (%; bottom). Results are obtained from quantification of five images in three independent experiments. (*C*) Trans-endothelial resistance in ORPK and IFT88* ECs. Mean ± SD. Results are obtained from seven independent experiments. *$P \leq 0.05$; **$P \leq 0.01$; ****$P \leq 0.0001$. Comparison of means, medians, and distributions has been performed using unpaired *t*-test, non-parametric Mann–Whitney *U*- and chi-square test, respectively. NA = not applicable.

Table 1 Demographic and clinical data of patients from the @neurIST study

Basic characteristics	Non-PKD patients	PKD patients	*P*-value
Patients	***N* = 904**	***N* = 21**	
Age, years: mean ± SD	54.9 ± 14.4	55.1 ± 18.4	0.97
Sex, female: *N* (%)	663 (73.3)	16 (76.2)	0.54
Smoker (current and former): *N* (%)	440 (48.7)	10 (47.6)	0.91
Hypertension: *N* (%)	353 (39.0)	13 (61.9)	0.02
Positive familial history: *N* (%)	107 (11.8)	7 (33.3)	0.01
Multiple IAs: *N* (%)	212 (23.5)	10 (47.6)	0.02

Comparisons of means and percentages have been performed using two-tailed non-paired Student's *t*-test and Fisher's exact test, respectively.
SD, standard deviation.

in collagen type towards more type I collagen and less type III collagen, and displayed a more degraded vascular wall phenotype. These histological changes in PKD aneurysms were comparable to those described for ruptured IAs when compared to non-ruptured IAs.[13] Finally, ECs in IA domes from PKD patients displayed lower ZO-1 levels compared to ECs of IA domes of non-PKD patients (*Figure 5*).

WSS is considered as an important driver of IA disease. Substantial evidence supports that aneurysmal remodelling starts when high WSS in combination with high positive WSS gradients goes beyond a certain threshold,[2–4] causing injury to the endothelium, disruption of the IEL, and loss of SMCs. Furthermore, it appeared that both low and high WSS could drive the growth of IAs.[4] In fact, low WSS in combination with high oscillatory shear index has been associated with inflammatory cell-mediated destructive remodelling, while high WSS and a positive WSS gradient cause mural cell-mediated remodelling.[4] Nevertheless, only few IAs rupture during a lifetime. It is therefore essential to understand how WSS relates to tissue changes leading to IA growth and rupture. The response of ECs to flow is mediated by mechano-sensors such as primary cilia. Genetic diseases characterized by absence or dysfunction of primary cilia, such as PKD, have been associated with increased risk of developing vascular disorders. In this study, we show that loss of primary cilia in ECs impaired the levels and organization of junction proteins. The latter effect may involve microtubule disassembly since they participate in trafficking of TJ proteins.[24] Indeed, loss of IFT88 has been associated with hyper-acetylation of microtubules altering microtubule stability.[25] An alternative mechanism may involve endothelial-to-mesenchymal transition (EndMT). It is known that the lack of primary cilia promotes EndMT through the control of the transcription factor SLUG.[14,26] Interestingly, SLUG has been associated with reduced expression of TJ proteins.[27] We hypothesized that primary cilia-induced junction remodelling would be mediated by ZO-1 as a central regulator. Targeting ZO-1 in wild-type ciliated ECs induced a shift towards a wider and discontinuous distribution of multiple junction proteins (*Figure 3*). Moreover, rescue of primary cilia in ECs resulted in increased ZO-1 expression and improved structural arrangement of cell–cell junctions (*Figure 4*). Interestingly, it has been demonstrated that irregular and diffuse junctions between ECs are associated to lower TEER,[28] hence supporting our findings.

Observations in different studies support a role of ZO-1 as key regulator of intercellular junctions. Thus, the absence of ZO-1 induced defects in vascular development with impaired formation of vascular trees, demonstrating the absolute requirement of ZO-1 in intercellular junction establishment and maintenance.[29] In addition, ZO-1 can regulate gene expression through its interaction with ZONAB.[30] ZO-1 has also the ability to translocate into the nucleus even though its function at this location has not yet been understood.[30,31] At an early stage of junction formation, ZO-1 is found at AJs and concentrates later at TJs.[32] ZO-1 recruitment and distribution along the intercellular border permits the recruitment and insertion of claudins and occludin to the cell membrane.[33] Finally, ZO-1 can regulate the rate of Cx43 accumulation at GJs.[34] The interaction of ZO-1 with its associated junction proteins is mediated through its PDZ domain.[30,35] A reduction of ZO-1 content would thus generate a competition for its PDZ domain and result in reduced or a less sharp intercellular localization of junction proteins with the lowest affinity.

ZO-1 activates multiple pathways crucial for endothelial junction homeostasis. For instance, it controls junctional tension by regulating molecular interactions of VE-cadherin complex to the force-generating cytoskeletal machinery but it also regulates endothelial barrier formation by influencing Claudin-5 expression.[36] The rescue of primary cilia did not restore Claudin-3 expression level in $Tg737^{orpk/orpk}$–Ift88* ECs (*Figure 4A and B*). In addition, we observed that the rescue of primary cilia only modestly improved TEER in $Tg737^{orpk/orpk}$–Ift88* ECs (*Figure 4C*), which suggests an important role for Claudin-3 in the *in vitro* endothelial barrier function of our EC model. We were unable to stain the paraffin-embedded human samples for Claudin-3 using presently available antibodies; however, potential differences in expression of claudins in the endothelium of IA domes between non-PKD and PKD patients are of particular interest and merit further investigation.

IA incidence[37] and the frequency of their rupture[38] are higher in PKD patients than in the general population, raising the question of a tailored screen for IA stability in this patient population. We have shown that the decrease of ZO-1 observed in ECs lacking primary cilia leads to an increased permeability for a large fluorescent tracer. In analogy, one might expect that contrast agents used for radiological imaging may display more diffuse distribution patterns due to leakiness of the endothelium in IAs of PKD patients. Interestingly, vessel wall contrast enhancement on magnetic resonance imaging visualizing the local accumulation of a colloid contrast agent is considered a promising tool for clinical staging of IA disease.[39–41] Even if the association with IA instability has been demonstrated,[42] the biological and radiological mechanisms resulting in vessel wall enhancement are presently unclear. Although a limitation of our study is that we have investigated the differential gene expression and function of ECs in an *in vitro* model, this reductionist approach helped to understand some of the mechano-transduction events occurring in the endothelium devoid of primary cilia. Future work using mutant animal models will shed some light on the role of primary cilia, ZO-1, and junctional organization in the pathogenesis of IAs. Such work will also allow

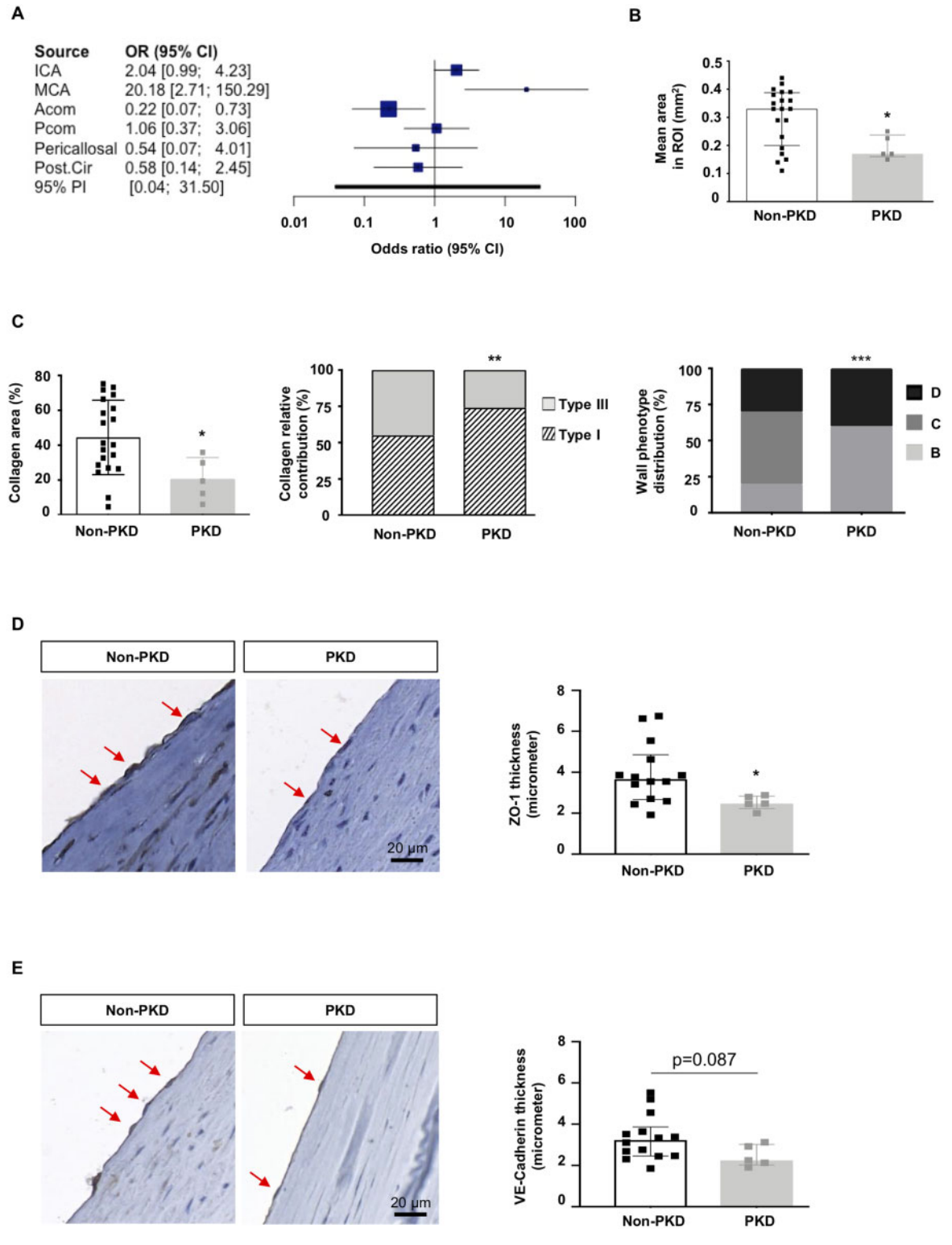

Figure 5 Characterization of IA domes of PKD and non-PKD patients. (*A*) Distribution and likelihood ratio of IA distribution between PKD and non-PKD patient groups (925 patients with 1076 IAs). (*B*) Mean surface area, measured in three to four regions of interest (ROI) covering almost the entire surface of the PKD ($N = 5$) and non-PKD ($N = 20$) IA dome sample. Median ± IQR. (*C*) Total collagen (left), relative distribution of type I and III collagen (middle), and distribution of severity grades (right) in PKD ($N = 5$) and non-PKD ($N = 20$) IA dome samples. Median ± IQR (left) or % (middle, right). (*D*) ZO-1 immunostaining (left images; in brown, some positive ECs are indicated by arrow) and quantification (right, Median ± IQR) on PKD ($N = 5$) and non-PKD ($N = 14$) IA dome samples. (*E*) VE-cadherin immunostaining (left images; in brown, some positive ECs are indicated by arrow) and quantification (right, Median ± IQR) on PKD ($N = 5$) and non-PKD ($N = 14$) IA dome samples. *$P < 0.05$; **$P < 0.01$; ***$P \leq 0.001$. Comparison of medians and distributions has been performed using non-parametric Mann–Whitney *U*-test and chi-square test, respectively.

Table 2 Patient and IA characteristics related to the AneuX biobank samples

	Non-PKD patients	PKD patients	*P*-value
Patients	*N* = 20	*N* = 4	
Age, years: median (IQR)	55 (48–64)	47 (40–67)	0.49
Sex, female: *N* (%)	15 (75)	2 (50)	NA
Smoker (former and current): *N* (%)	14 (70)	2 (50)	NA
Hypertension: *N* (%)	8 (40)	4 (100)	NA
Positive familial history: *N* (%)	3 (15)	2 (67)	NA
Multiple aneurysms: *N* (%)	11 (55)	2 (50)	NA
Intracranial aneurysms	*N* = 20	*N* = 5	
Rough appearance: *N* (%)	11 (58)	1 (20)	NA
Presence of blebs or lobules: *N* (%)	11 (55)	1 (20)	NA
Neck size, mm: median (IQR)	4.2 (3.2–5.5)	2.8 (2.5–3.8)	0.03
Maximal diameter, mm: median (IQR)	6.3 (5.4–9.9)	3.7 (2.4–5.6)	0.01
Bottleneck factor: median (IQR)	1.6 (1.2–1.9)	1.1 (0.9–1.6)	0.11

Comparisons of medians have been performed using non-parametric Mann–Whitney *U*-test.
Bottleneck factor = maximum diameter/neck size; IQR, interquartile range; NA, not applicable.

for linking vessel wall imaging directly to vessel wall function and histology. Moreover, further research should also provide insight whether the signalling pathways identified with the help of this PKD cell model may be generalized to the endothelium of instable IAs, thus allowing for the development of biomarkers or radiological tracers for vulnerable IAs.

Supplementary material

Supplementary material is available at *Cardiovascular Research* online.

Acknowledgements

We thank Bernard Foglia, Graziano Pelli, and Esther Sutter for excellent technical assistance.

Funding

This study was supported by grants from the Swiss SystemsX.ch Initiative, evaluated by the Swiss National Science Foundation [to P.B. and B.R.K.], the Swiss National Science Foundation [310030_162579 to B.R.K.], the Swiss Heart Foundation [to B.R.K. and P.B.], the Gottfried und Julia Bangerter-Rhyner-Stiftung [to B.R.K.], the Novartis Foundation for Medical-Biological Research [to B.R.K.], and the Fondation Privée des HUG [to B.R.K., P.B., and E.A.].

Conflict of interest: None declared.

Data availability

The data underlying this article are available in the article and in its Supplementary material online. RNA sequencing data have been submitted to GEO database under accession number GSE139580.

References

1. Brisman JL, Song JK, Newell DW. Cerebral aneurysms. *N Engl J Med* 2006;**355**:928–939.
2. Diagbouga MR, Morel S, Bijlenga P, Kwak BR. Role of hemodynamics in initiation/growth of intracranial aneurysms. *Eur J Clin Invest* 2018;**48**:e12992.
3. Frosen J, Cebral J, Robertson AM, Aoki T. Flow-induced, inflammation-mediated arterial wall remodeling in the formation and progression of intracranial aneurysms. *Neurosurg Focus* 2019;**47**:E21.
4. Meng H, Tutino VM, Xiang J, Siddiqui A. High WSS or low WSS? Complex interactions of hemodynamics with intracranial aneurysm initiation, growth, and rupture: toward a unifying hypothesis. *AJNR Am J Neuroradiol* 2014;**35**:1254–1262.
5. Kwak BR, Back M, Bochaton-Piallat ML, Caligiuri G, Daemen MJ, Davies PF, Hoefer IE, Holvoet P, Jo H, Krams R, Lehoux S, Monaco C, Steffens S, Virmani R, Weber C, Wentzel JJ, Evans PC. Biomechanical factors in atherosclerosis: mechanisms and clinical implications. *Eur Heart J* 2014;**35**:3013–3020.
6. Aoki T, Kataoka H, Shimamura M, Nakagami H, Wakayama K, Moriwaki T, Ishibashi R, Nozaki K, Morishita R, Hashimoto N. NF-kappaB is a key mediator of cerebral aneurysm formation. *Circulation* 2007;**116**:2830–2840.
7. Krishnappa V, Vinod P, Deverakonda D, Raina R. Autosomal dominant polycystic kidney disease and the heart and brain. *Cleve Clin J Med* 2017;**84**:471–481.
8. Zhou S, Dion PA, Rouleau GA. Genetics of intracranial aneurysms. *Stroke* 2018;**49**:780–787.
9. Brown JM, Witman GB. Cilia and diseases. *Bioscience* 2014;**64**:1126–1137.
10. Nauli SM, Kawanabe Y, Kaminski JJ, Pearce WJ, Ingber DE, Zhou J. Endothelial cilia are fluid shear sensors that regulate calcium signaling and nitric oxide production through polycystin-1. *Circulation* 2008;**117**:1161–1171.
11. Van der Heiden K, Hierck BP, Krams R, de Crom R, Cheng C, Baiker M, Pourquie MJ, Alkemade FE, DeRuiter MC, Gittenberger-de Groot AC, Poelmann RE. Endothelial primary cilia in areas of disturbed flow are at the base of atherosclerosis. *Atherosclerosis* 2008;**196**:542–550.
12. Liu M, Zhao J, Zhou Q, Peng Y, Zhou Y, Jiang Y. Primary cilia deficiency induces intracranial aneurysm. *Shock* 2018;**49**:604–611.
13. Morel S, Diagbouga MR, Dupuy N, Sutter E, Braunersreuther V, Pelli G, Corniola M, Gondar R, Jagersberg M, Isidor N, Schaller K, Bochaton-Piallat ML, Bijlenga P, Kwak BR. Correlating clinical risk factors and histological features in ruptured and unruptured human intracranial aneurysms: the Swiss AneuX Study. *J Neuropathol Exp Neurol* 2018;**77**:555–566.
14. Egorova AD, Khedoe PP, Goumans MJ, Yoder BK, Nauli SM, ten Dijke P, Poelmann RE, Hierck BP. Lack of primary cilia primes shear-induced endothelial-to-mesenchymal transition. *Circ Res* 2011;**108**:1093–1101.
15. Pfenniger A, Wong C, Sutter E, Cuhlmann S, Dunoyer-Geindre S, Mach F, Horrevoets AJ, Evans PC, Krams R, Kwak BR. Shear stress modulates the expression of the atheroprotective protein Cx37 in endothelial cells. *J Mol Cell Cardiol* 2012;**53**:299–309.
16. Sabine A, Bovay E, Demir CS, Kimura W, Jaquet M, Agalarov Y, Zangger N, Scallan JP, Graber W, Gulpinar E, Kwak BR, Makinen T, Martinez-Corral I, Ortega S, Delorenzi M, Kiefer F, Davis MJ, Djonov V, Miura N, Petrova TV. FOXC2 and fluid shear stress stabilize postnatal lymphatic vasculature. *J Clin Invest* 2015;**125**:3861–3877.
17. Skalli O, Ropraz P, Trzeciak A, Benzonana G, Gillessen D, Gabbiani G. A monoclonal antibody against alpha-smooth muscle actin: a new probe for smooth muscle differentiation. *J Cell Biol* 1986;**103**:2787–2796.
18. Dobin A, Davis CA, Schlesinger F, Drenkow J, Zaleski C, Jha S, Batut P, Chaisson M, Gingeras TR. STAR: ultrafast universal RNA-seq aligner. *Bioinformatics* 2013;**29**:15–21.

19. Quinlan AR, Hall IM. BEDTools: a flexible suite of utilities for comparing genomic features. *Bioinformatics* 2010;**26**:841–842.
20. Robinson MD, McCarthy DJ, Smyth GK. edgeR: a Bioconductor package for differential expression analysis of digital gene expression data. *Bioinformatics* 2010;**26**:139–140.
21. RC Team. R: A Language and Environment for Statistical Computing. Vienna, Austria: R Foundation for Statistical Computing; 2011.
22. Bazzoni G, Dejana E. Endothelial cell-to-cell junctions: molecular organization and role in vascular homeostasis. *Physiol Rev* 2004;**84**:869–901.
23. FröSen J, Piippo A, Paetau A, Kangasniemi M, Niemelä M, Hernesniemi J, JäÄSkeläInen J, Remodeling of saccular cerebral artery aneurysm wall is associated with rupture: histological analysis of 24 unruptured and 42 ruptured cases. *Stroke* 2004;**35**:2287–2293.
24. Glotfelty LG, Zahs A, Iancu C, Shen L, Hecht GA. Microtubules are required for efficient epithelial tight junction homeostasis and restoration. *Am J Physiol Cell Physiol* 2014;**307**:C245–C254.
25. Berbari NF, Sharma N, Malarkey EB, Pieczynski JN, Boddu R, Gaertig J, Guay-Woodford L, Yoder BK. Microtubule modifications and stability are altered by cilia perturbation and in cystic kidney disease. *Cytoskeleton (Hoboken)* 2013;**70**:24–31.
26. Sánchez-Duffhues G, de Vinuesa AG, Lindeman JH, Mulder-Stapel A, DeRuiter MC, Van Munsteren C, Goumans M-J, Hierck BP, Ten Dijke P. Ten Dijke P. SLUG is expressed in endothelial cells lacking primary cilia to promote cellular calcification. *Arterioscler Thromb Vasc Biol* 2015;**35**:616–627.
27. Wang Z, Wade P, Mandell KJ, Akyildiz A, Parkos CA, Mrsny RJ, Nusrat A. Raf 1 represses expression of the tight junction protein occludin via activation of the zinc-finger transcription factor slug. *Oncogene* 2007;**26**:1222–1230.
28. Hilfenhaus G, Nguyen DP, Freshman J, Prajapati D, Ma F, Song D, Ziyad S, Cuadrado M, Pellegrini M, Bustelo XR, Iruela-Arispe ML. Vav3-induced cytoskeletal dynamics contribute to heterotypic properties of endothelial barriers. *J Cell Biol* 2018;**217**:2813–2830.
29. Dejana E. Endothelial cell-cell junctions: happy together. *Nat Rev Mol Cell Biol* 2004;**5**:261–270.
30. González-Mariscal L, Domínguez-Calderón A, Raya-Sandino A, Ortega-Olvera JM, Vargas-Sierra O, Martínez-Revollar G. Tight junctions and the regulation of gene expression. *Semin Cell Dev Biol* 2014;**36**:213–223.
31. Gottardi CJ, Arpin M, Fanning AS, Louvard D. The junction-associated protein, zonula occludens-1, localizes to the nucleus before the maturation and during the remodeling of cell-cell contacts. *Proc Natl Acad Sci USA* 1996;**93**:10779–10784.
32. Itoh M, Nagafuchi A, Yonemura S, Kitani-Yasuda T, Tsukita S, Tsukita S. The 220-kD protein colocalizing with cadherins in non-epithelial cells is identical to ZO-1, a tight junction-associated protein in epithelial cells: cDNA cloning and immunoelectron microscopy. *J Cell Biol* 1993;**121**:491–502.
33. Fanning AS, Anderson JM. Zonula occludens-1 and -2 are cytosolic scaffolds that regulate the assembly of cellular junctions. *Ann N Y Acad Sci* 2009;**1165**:113–120.
34. Hunter AW, Barker RJ, Zhu C, Gourdie RG. Zonula occludens-1 alters connexin43 gap junction size and organization by influencing channel accretion. *Mol Biol Cell* 2005;**16**:5686–5698.
35. Nomme J, Antanasijevic A, Caffrey M, Van Itallie CM, Anderson JM, Fanning AS, Lavie A. Structural basis of a key factor regulating the affinity between the zonula occludens first PDZ domain and claudins. *J Biol Chem* 2015;**290**:16595–16606.
36. Tornavaca O, Chia M, Dufton N, Almagro LO, Conway DE, Randi AM, Schwartz MA, Matter K, Balda MS. ZO-1 controls endothelial adherens junctions, cell-cell tension, angiogenesis, and barrier formation. *J Cell Biol* 2015;**208**:821–838.
37. Kuo IY, Chapman A. Intracranial aneurysms in ADPKD how far have we come? *CJASN* 2019;**14**:1119–1121.
38. Sanchis IM, Shukoor S, Irazabal MV, Madsen CD, Chebib FT, Hogan MC, El-Zoghby Z, Harris PC, Huston J, Brown RD, Torres VE. Presymptomatic screening for intracranial aneurysms in patients with autosomal dominant polycystic kidney disease. *CJASN* 2019;**14**:1151–1160.
39. Samaniego EA, Roa JA, Hasan D. Vessel wall imaging in intracranial aneurysms. *J Neurointerv Surg* 2019;**11**:1105–1112.
40. Texakalidis P, Hilditch CA, Lehman V, Lanzino G, Pereira VM, Brinjikji W. Vessel wall imaging of intracranial aneurysms: systematic review and meta-analysis. *World Neurosurg* 2018;**117**:453–458.
41. Wang X, Zhu C, Leng Y, Degnan AJ, Lu J. Intracranial aneurysm wall enhancement associated with aneurysm rupture: a systematic review and meta-analysis. *Acad Radiol* 2019;**26**:664–673.
42. Matouk CC, Mandell DM, Gunel M, Bulsara KR, Malhotra A, Hebert R, Johnson MH, Mikulis DJ, Minja FJ. Vessel wall magnetic resonance imaging identifies the site of rupture in patients with multiple intracranial aneurysms: proof of principle. *Neurosurgery* 2013;**72**:492–496.

Translational Perspective

Intracranial aneurysms (IAs) are relatively common, with a prevalence of 4%. Most IAs are asymptomatic, but their rupture causes subarachnoid haemorrhage, a life-threatening event. Polycystic kidney disease (PKD) patients, who have abnormal or no primary cilia, are more prone to develop IAs with a prevalence up to 40%. We show here that primary cilia dampen the endothelial response to aneurysmal low wall shear stress. In absence of primary cilia, ZO-1 expression levels are reduced, which disorganizes intercellular junctions resulting in increased endothelial permeability. This altered endothelial function may not only contribute to the severity of IA disease observed in PKD patients, but may also serve as a potential diagnostic tool to determine the vulnerability of IAs.